Available online at www.sciencedirect.com
SCIENCE DIRECT
Journal of Catalysis 232 (2005) 102–107
JOURNAL OF CATALYSIS
www.elsevier.com/locate/jcat

The relationship between photocatalytic activity and crystal structure in strontium tantalates

Kohtaro Yoshioka [a], Valery Petrykin [b], Masato Kakihana [b,*], Hideki Kato [c], Akihiko Kudo [c,d]

[a] *Materials and Structures Laboratory, Tokyo Institute of Technology, 4259 Nagatsuta, Midori-ku, Yokohama 226-8503, Japan*
[b] *Institute of Multidisciplinary Research for Advanced Materials, Tohoku University, Katahira 2-1-1, Aoba-ku, Sendai 980-8577, Japan*
[c] *Department of Applied Chemistry, Faculty of Science, Science University of Tokyo, 1-3 Kagurazaka, Shinjyuku-ku, Tokyo 162-8601, Japan*
[d] *Core Research for Evolutional Science and Technology, Japan Science and Technology Agency (CREST, JST), 4-1-8 Honcho, Kawaguchi-shi, Saitama 332-0012, Japan*

Received 22 November 2004; revised 3 February 2005; accepted 22 February 2005

Available online 7 April 2005

Abstract

Three compounds, $SrTa_2O_6$, $Sr_4Ta_2O_9$, and $Sr_5Ta_4O_{15}$, were synthesized by a polymerizable complex method. Their photocatalytic activities for water splitting into H_2 and O_2 were tested and compared against previously published results for $Sr_2Ta_2O_7$. It was found that the efficiency of the catalysts decreases in the following order: $Sr_2Ta_2O_7 > Sr_5Ta_4O_{15} > SrTa_2O_6 > Sr_4Ta_2O_9$. The relationship between photocatalytic activities and crystal structures is discussed.

Keywords: Polymerizable complex method; Photocatalytic water splitting; SrTaO system

1. Introduction

Among various important reactions, the photoinduced decomposition of water into H_2 and O_2 is potentially one of the most promising means of converting photon energy into chemical energy [1]. In the recent years a broad range of complex oxides that include tantalum were reported to exhibit very high photocatalytic activities for water decomposition. Although complex tantalates such as $K_3Ta_3Si_2O_{13}$ [2], $ATaO_3$ (A = Li, Na, K) [3,4], $Sr_2Ta_2O_7$ [5], $RbLnTa_2O_7$ [6], $K_2LnTa_5O_{15}$ [7], $A_2SrTa_2O_7 \cdot nH_2O$ (A = H, K, Rb) [8], etc. have quite different chemical compositions and crystal structures, they share a common feature: the TaO_6 octahedra interconnected in the one-, two- or three-dimensional manner.

The vast majority of methods of powder synthesis of these tantalates have been carried out to date with the conventional solid-state reaction (SSR) route at high temperatures (typically 1273–1573 K). Common problems in the SSR route include uncontrollable grain growth, segregation of one or more components, and possible loss of stoichiometry due to volatilization of the constituent components at high temperatures, all of which result in a great decrease in the photocatalytic activity of the catalyst. Considering the need to obtain pure and homogeneous crystalline powders with high surface areas for catalytic applications, solution processing is expected to be satisfactory and the best adapted method. We have previously utilized the Pechini-type polymerizable complex (PC) route [9,10], based upon polyesterification between citric acid and ethylene glycol for synthesis of photocatalysts with improved activities for the decomposition of water. The most remarkable activity has been achieved for $Sr_2Ta_2O_7$ [11].

$Sr_2Ta_2O_7$ has been synthesized so far by the SSR method at 1453 K for 200 h [5] and by the PC method at 1073 K for 48 h [11]. The specific surface area of $Sr_2Ta_2O_7$ synthesized by the PC method was 10.7 $m^2\ g^{-1}$, which is 12 times higher than that observed for the SSR method, 0.9 $m^2\ g^{-1}$ [11]. In the Sr–Ta–O system three other potentially interesting com-

* Corresponding author. Fax: +81 22 217 5649.
E-mail address: kakihana@tagen.tohoku.ac.jp (M. Kakihana).

0021-9517/$ – see front matter
doi:10.1016/j.jcat.2005.02.021

pounds may form, $SrTa_2O_6$, $Sr_5Ta_4O_{15}$, and $Sr_6Ta_2O_{11}$ [12], and they may be prospective photocatalysts. $SrTa_2O_6$ has been synthesized by the SSR flux method at 1373 K for 10 h [13], and the PC method was successfully applied to its synthesis at 1273 K for 12 h without the flux. $Sr_5Ta_4O_{15}$ has never been obtained in the pure form with the SSR method [14]. Therefore its crystal structure has not been determined until now, although one may assume it should be isostructural to the known $Ba_5Ta_4O_{15}$ phase [14]. The lattice parameters of the last compound in this system, $Sr_6Ta_2O_{11}$, correspond with the cubic phase with $a = 8.34$ Å [12] and indicate that in reality it might be the recently reported compound $Sr_{1.4}Ta_{0.6}O_{2.9}$ [15], which has the crystal structure of the $A(A_{1/3}B_{2/3})O_3$ perovskite. Consequently its ideal composition should be close to $Sr_4Ta_2O_9$. Reports of $Sr_4Ta_2O_9$ synthesis have not been published; however, the compounds of such stoichiometry are known in Ba–Ta–O [16] and Sr–Nb–O [17] systems.

The principal aim of this paper is to study the relationship between the photocatalytic activity and the crystal structures of $SrTa_2O_6$, $Sr_4Ta_2O_9$, and $Sr_5Ta_4O_{15}$ ($Sr_mTa_nO_{(m+5n/2)}$) compounds prepared by the PC method at reduced temperatures. The photocatalytic decomposition of water into H_2 and O_2 over these materials with a NiO co-catalyst was considered as a model process.

2. Experimental

Powders of $Sr_mTa_nO_{(m+5n/2)}$ were synthesized by the PC method as schematically described in Fig. 1. After $TaCl_5$ was dissolved in methanol, anhydrous citric acid (CA) and ethylene glycol (EG) with Ta/CA/EG = 1/15/60 ratio were added. The solution was magnetically stirred for 20 min at 373 K, followed by the addition of $SrCO_3$. After $SrCO_3$ dissolved completely, the obtained solution has been kept at 473 K for several hours to promote polymerization to obtain a polymeric gel. It is important that no visible formation of precipitation or turbidity was observed during the polymerization and after gel formation. The gel was pyrolyzed at 723 K to form powder precursors. $SrTa_2O_6$, $Sr_4Ta_2O_9$, and $Sr_5Ta_4O_{15}$ were subsequently heat-treated in a furnace at 1273 K in air for 12, 12, and 60 h, respectively.

$Sr_mTa_nO_{(m+5n/2)}$ materials loaded with 0.15 wt% NiO were prepared by the impregnation of powders of the host $Sr_mTa_nO_{(m+5n/2)}$ compounds with aqueous solutions of nickel nitrate, followed by appropriate heat treatments [18]. Powders of $Sr_mTa_nO_{(m+5n/2)}$ prepared by the PC method were suspended in an aqueous solution containing $Ni(NO_3)_2$ with a required amount, and water was evaporated on a water bath. The residue was dried at 373 K for 10 h in a drying oven. Then the powder was heat-treated at 643 K in a furnace for 1 h.

The final products were characterized by X-ray diffraction (XRD) with a scanning speed of $4^\circ\,\mathrm{min}^{-1}$ for phase identification with a Mac Science MXP 3VA. Cu-K_α radiation ($\lambda = 1.540562$ Å) was used. The diffraction patterns for Rietveld analysis were collected in the step-scanning mode (step = 0.02°, counting time = 2 s step^{-1}). Rietan [19] was used for Rietveld structural refinement. Ultraviolet–visible (UV–vis) diffuse reflectance spectra were measured for the products with a Shimadzu UV-3100PC spectrometer, and they were converted from reflection to absorbance through the standard Kubelka–Munk method. Specific surface areas were measured by the gas adsorption method with a Shimadzu TriStar3000. Nitrogen gas was used as an adsorption gas. Photocatalytic reactions were carried out in a closed-gas circulation system. The powdered photocatalysts (0.5 g of each) were magnetically suspended in 390 ml of pure water in an inner irradiation quartz cell. After thorough degassing, Ar (60–80 Torr) was introduced into the cell. The photodecomposition of water was then carried out under irradiation of light from a high-pressure 400-W Hg lamp (SEN, HL-400EH-5). The H_2/O_2 gases that evolved were analyzed by gas chromatography (Shimadzu, GC-8A, Ar gas carrier, MS-5A Column, TCD).

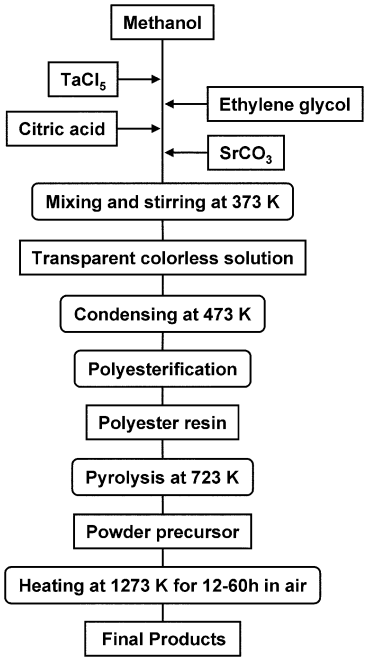

Fig. 1. Flow chart of preparing $Sr_mTa_nO_{(m+5n/2)}$ compounds by the polymerizable complex method.

3. Results and discussion

3.1. Synthesis and characterization

The single phase of $SrTa_2O_6$ was obtained after the final annealing at 1273 K for 12 h. All peaks on the diffraction pattern can be indexed as belonging to the orthorhombic unit cell with $a = 11.0048(4)$ Å, $b = 7.6318(3)$ Å, and $c = 5.6234(2)$ Å, which is in good agreement with its re-

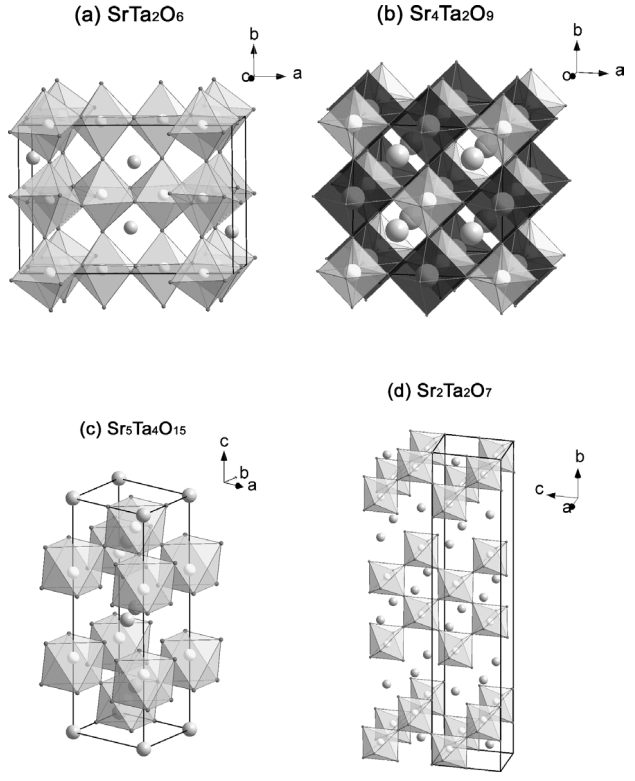

Fig. 2. Crystal structure images of $Sr_mTa_nO_{(m+5n/2)}$: (a) $SrTa_2O_6$ [12], (b) $Sr_4Ta_2O_9$, (c) $Sr_5Ta_4O_{15}$, (d) $Sr_2Ta_2O_7$ [28].

ported structure [20]. The crystal structure of $SrTa_2O_6$ is displayed in Fig. 2a.

The XRD pattern of $Sr_4Ta_2O_9$ after the synthesis at 1273 K for 12 h could be indexed as a cubic cell with $a = 8.2725(9)$ Å and a hexagonal unit cell with $a = 5.8566(3)$ Å, $c = 14.3212(7)$ Å with very close merit factors. Surprisingly, one may find literature data supporting each of these results. In the first case the cubic phase corresponds to the $Sr_{1.4}Ta_{0.6}O_{2.9}$ phase with a perovskite-type arrangement of MeO_6 octahedra, as described by Caldes [15]. In the second case the hexagonal unit cell may indicate the formation of the compound isostructural to $Ba_3SrTa_2O_9$ [21], which has pairs of face-sharing octahedra connected by corner-sharing. Keeping in mind the polymorphism in $Ba_4Ta_2O_9$, one may suspect the existence of both cubic and hexagonal phases in the prepared sample. To identify the main phase and to determine the mass fraction of each phase (if both phases are present), we have carried out analysis of the diffraction pattern by the Rietveld method. It was found that only the cubic $Sr_4Ta_2O_9$ phase was present in the sample, and its structural parameters agree well with the crystal structure reported by Caldes [15]. The result of Reitveld refinement (observed, simulated patterns and difference) is shown in Fig. 3. It gave the refined value of cubic phase lattice parameter $a = 8.27107(8)$ Å and good reliability factors of $S = 1.17$, $R_{wp} = 11.62\%$, $R_p = 8.62\%$, $R_e = 9.94\%$, $R_B = 3.77\%$, $R_F = 3.60\%$. The crystal structure of the $Sr_4Ta_2O_9$ phase is displayed in Fig. 2b. This

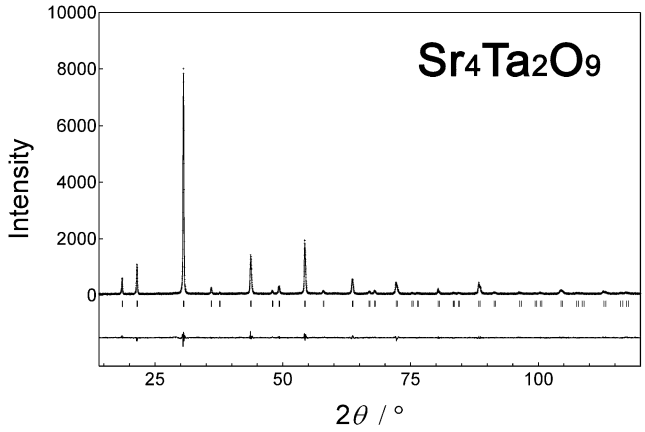

Fig. 3. Experimental (dotted line) and calculated (line) X-ray powder diffraction profiles of $Sr_4Ta_2O_9$. Lower line is the residual.

Table 1
Refined structure parameters of $Sr_5Ta_4O_{15}$

Atom	Site	x	y	z	ADP (Å^2)
Sr1	1a	0	0	0	0.34
Sr2	2d	1/3	2/3	0.78311(36)	0.34
Sr3	2d	1/3	2/3	0.44799(38)	0.34
Ta1	2c	0	0	0.68216(12)	0.71
Ta2	2d	1/3	2/3	0.10487(7)	0.71
O1	3e	1/2	0	0	0.77
O2	6i	0.17000(16)	−0.17000(16)	0.19400(12)	1.43
O3	6i	0.16766(19)	−0.16926(19)	0.60568(27)	0.47

Space group is P-3m1, $a = 5.65406(4)$ Å, $c = 11.4944(1)$ Å, $S = 1.09$, $R_{wp} = 8.51\%$, $R_p = 6.03\%$, $R_e = 7.79\%$, $R_B = 3.81\%$, $R_F = 3.38\%$

structure is derived from the cubic perovskite with "rock-salt-like" ordering of TaO_6 and $(Sr_{2/3}/Ta_{1/3})O_6$ octahedra.

The structural data for $Sr_5Ta_4O_{15}$ have not been published; therefore we attempted to characterize it ourselves. Its diffraction pattern could be indexed as that of the hexagonal unit cell ($a = 5.6545(2)$ Å, $c = 11.4942(5)$ Å). Since the extinction rules and the relative peak intensities were similar to the reported structure of the $Ba_5Ta_4O_{15}$ compound [22], we used its space group and atomic positions as a starting model for the refinement. The result of the final refinement circle is presented in Table 1. Fig. 4 demonstrates the observed, calculated, and residual patterns after the final stage of refinement. The difference Fourier map did not reveal any additional atoms or/and atoms placed in the wrong site. The estimated bond valence sums (BVS) [23] of Sr and Ta ($BVS_{Sr1} = 1.88$, $BVS_{Sr2} = 1.95$, $BVS_{Sr3} = 2.13$, $BVS_{Ta1} = 4.95$, $BVS_{Ta2} = 5.40$) are close to their expected valence state, indicating their reasonable coordination environment. The refined crystal structure of $Sr_5Ta_4O_{15}$ is displayed in Fig. 2c.

Diffuse reflection spectra for $SrTa_2O_6$, $Sr_4Ta_2O_9$, and $Sr_5Ta_4O_{15}$ prepared by the PC method are shown in Fig. 5. The band gaps of $SrTa_2O_6$, $Sr_4Ta_2O_9$, and $Sr_5Ta_4O_{15}$ were estimated to be 4.49, 4.81, and 4.75 eV, from the absorption edge wavelength for each UV–vis spectrum.

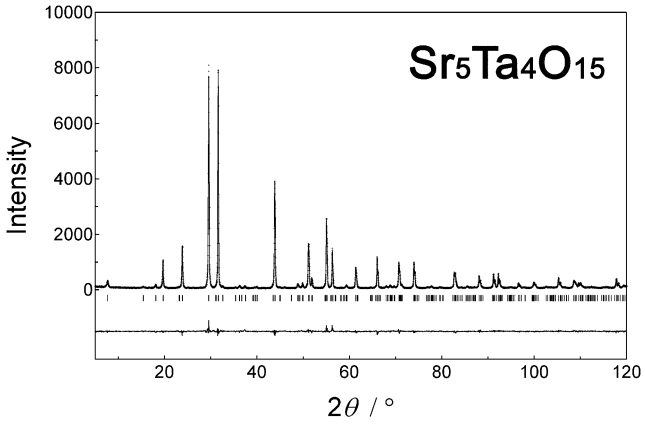

Fig. 4. Experimental (dotted line) and calculated (line) X-ray powder diffraction profiles of $Sr_5Ta_4O_{15}$. Lower line is the residual.

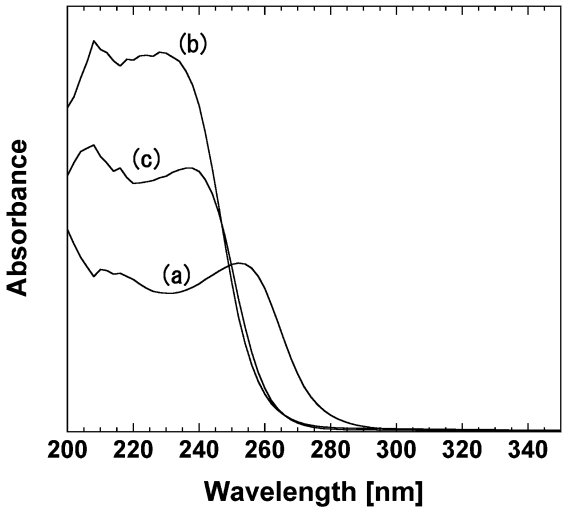

Fig. 5. Diffuse reflectance spectra of $Sr_mTa_nO_{(m+5n/2)}$: (a) $SrTa_2O_6$, (b) $Sr_4Ta_2O_9$, (c) $Sr_5Ta_4O_{15}$.

Table 2
Photocatalytic activities of NiO (0.15 wt%)/$Sr_mTa_nO_{(m+5n/2)}$ prepared by the polymerizable complex method

Catalyst	Surface area ($m^2\,g^{-1}$)	Calcination	H_2 (μmol)	O_2 (μmol)
$SrTa_2O_6$	3.94	1273 K, 12 h	394	202
$Sr_2Ta_2O_7$ [11]	4.5	1273 K, 5 h	2141	1059
$Sr_4Ta_2O_9$	2.61	1273 K, 12 h	32	2
$Sr_5Ta_4O_{15}$	2.99	1273 K, 60 h	1194	722

3.2. *Photocatalytic activities of NiO-loaded $Sr_mTa_nO_{(m+5n/2)}$*

Fig. 6 shows the time course of H_2 and O_2 evolution over NiO (0.15 wt%)/$Sr_mTa_nO_{(m+5n/2)}$. Table 2 compares photocatalytic activities (between 1 and 2 h) of NiO-loaded $Sr_mTa_nO_{(m+5n/2)}$ prepared by the PC method. In the series of the synthesized samples the highest activity of the photocatalytic splitting of water was exhibited by the $Sr_5Ta_4O_{15}$ sample. Nevertheless, its activity was approximately two

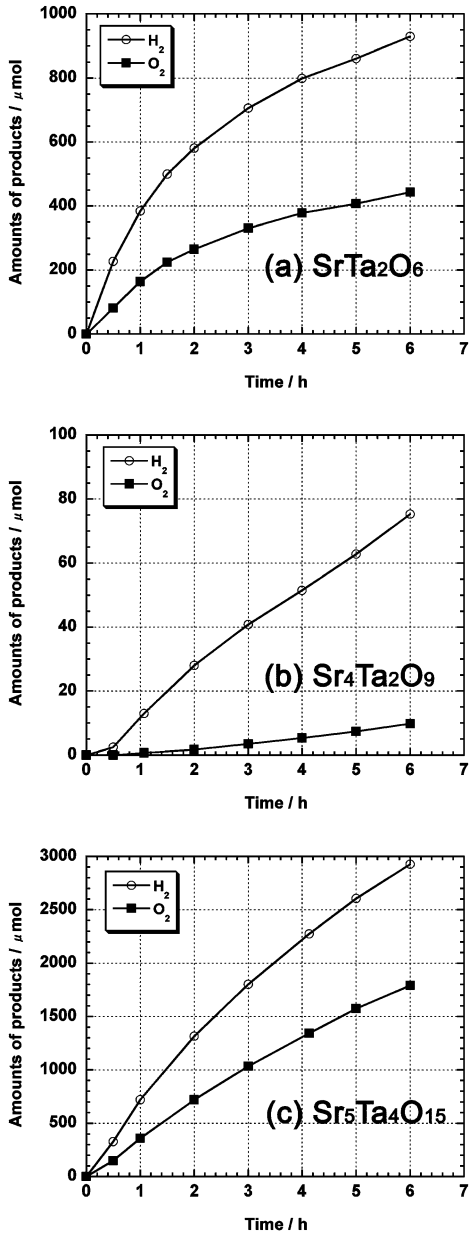

Fig. 6. Time course of H_2 and O_2 evolution from pure water over (a) NiO (0.15 wt%)/$SrTa_2O_6$, (b) NiO (0.15 wt%)/$Sr_4Ta_2O_9$, and NiO (0.15 wt%)/$Sr_5Ta_4O_{15}$ synthesized by the polymerizable complex method at 1273 K for 12 h, 1273 K for 12 h, and 1273 K for 60 h. Amounts of products are expressed in units per gram of catalyst.

times lower than the reported activity of $Sr_2Ta_2O_7$ [11] (see Table 2) prepared by a similar method. The second efficiency in the row was demonstrated by $SrTa_2O_6$, and $Sr_4Ta_2O_9$ was able to produce H_2 with the lowest rate among the $Sr_mTa_nO_{(m+5n/2)}$ materials. O_2 evolution in the case of $Sr_4Ta_2O_9$ was extremely small, and the ratio of the produced H_2/O_2 was less than expected from the stoichiometry. According to Wrighton et al. [24] the deficiency of the evolved O_2 from nonalkaline solutions in the course of the photoelectrochemical reaction can be accounted for almost fully by the formation of the competing product H_2O_2, which decomposes into water and oxygen after a considerable time.

3.3. The relation between the photocatalytic activity and the crystal structure

In $Sr_mTa_nO_{(m+5n/2)}$ compounds the valance band originates from the interaction of fully filled O2p bonding orbitals, and the conduction band results from the interaction of the Ta5d nonbonding orbitals (t_{2g}) in the TaO_6 octahedra arranged in the periodic crystal lattice [5]. The absorbed light with energy equal to or greater than the band-gap energy of the semiconductor excites electrons to the conduction band. Thus created conduction electrons and holes participate in the reaction with water on the surface of photocatalysts yielding H_2 and O_2. Scaife has studied the relationship between flat band potentials (V_{fb}) and band gaps (E_g) for oxide semiconductors without a partly filled d-level [25]. According to this reference, the top of the valence band in the oxide materials with d^0-elements is formed primarily by oxygen 2p orbitals interacting with d orbitals of the metal, and it is located approximately at 3 V with respect to the normal hydrogen electrode potential (−7.4 eV E_{vac} level). Then one may conclude that the bottom of the conduction bands for all of the considered compounds in this work should be at −1.6–1.9 V versus E(NHE) (more negative than H_2 evolution potential). Therefore the energy of the photogenerated electrons and holes should be sufficient for water splitting into H_2 and O_2 under UV irradiation with $Sr_mTa_nO_{(m+5n/2)}$, and this conclusion agrees with the experimental data on photocatalytic hydrogen and oxygen production by the prepared materials.

The photocatalytic activities for all of the samples were investigated with the use of a high-pressure mercury lamp for excitation. The emission spectrum of the same light source has been reported previously [26]. Considering the light absorption spectra (reflectivity data) for the synthesized samples and the emission spectrum of the Hg lamp [26], one should not expect a tremendous difference in the number of photogenerated electrons and holes that can account for a difference of several orders of magnitude in the hydrogen and oxygen evolution rate. And even if such a difference does exist, the following order of the photocatalytic activities will appear: $Sr_2Ta_2O_7 \approx SrTa_2O_6 > Sr_4Ta_2O_9 \approx Sr_5Ta_4O_{15}$. Though $Sr_2Ta_2O_7$ indeed seemed to be the most efficient photocatalyst in the Sr–Ta–O system, the trend expected purely from the band-gap energies does not explain the experimental activities of water splitting by the obtained materials. Thus we assumed that it is the crystal structure (and hence the peculiarities of the band structure) that determines the difference in the photocatalytic properties of these strontium tantalates.

The topology of the MO_6 bonding in the perovskites and related compounds and its effect on the electronic structure of these materials were recently reported by Eng et al. [27]. Their conclusions can be directly transferred to explain the photocatalytic behavior of $Sr_4Ta_2O_9$, $Sr_5Ta_4O_{15}$, and $Sr_2Ta_2O_7$ compounds in which TaO_6 is connected by corner-sharing. $Sr_4Ta_2O_9$ possesses the structure of the double perovskite (Fig. 2b), and TaO_6 octahedra, neighboring the diagonal of the cube face, give rise to an extremely narrow conduction band, which cannot provide efficient carrier migration. (To be precise, one should expect formation of "conducting chains" of random length due to the Ta substitution for Sr in the $(Sr_{2/3}/Ta_{1/3})O_6$; however, those chains will be terminated by "insulating" SrO_6 blocks.) In this case the band-gap energy of 4.81 eV estimated from the diffuse-reflectance spectrum corresponds almost exclusively to the excitation of an electron from the O2p orbital to the nonbonding t_{2g} orbital of Ta in the isolated TaO_6 octahedron [27]. Therefore, although the photocatalytic splitting of water by this material is possible from a thermodynamic viewpoint, it is essentially hindered by the nature of the conduction band in the double perovskite.

When considering the usual perovskites and related structural types with 2D perovskite-like blocks, Eng et al. [27] had concluded that transition from 3D to 2D does not lead to the serious differences in the energy of the band gap and width of the conduction band. What matters most is the deviation of the M–O–M bond angle from 180°. When the bond angle decreases, the conduction band becomes narrower and the band gap increases by the same amount. (It is worth the reader's attention to observe that the value of M–O–M bond angle and its deviation from 180° have been noticed to play a crucial role in photocatalyst performance [4,5].) Thus despite the different symmetry and slightly different atomic layer arrangement in $Sr_5Ta_4O_{15}$ and $Sr_2Ta_2O_7$ (Figs. 2c and d), the trend in the band-gap widths should reflect the difference in the conduction band width. From Fig. 5 and the reported band gap for $Sr_2Ta_2O_7$ [11], one may find that the band gap decreases in the series $Sr_4Ta_2O_9$, $Sr_5Ta_4O_{15}$, and $Sr_2Ta_2O_7$, and, consequently, the width of the conduction band increases in the same order. Therefore it is not surprising now that the photocatalytic activity of these materials exhibits the same trend (see Table 2).

On an intuitive level it can be understood that the infinite length of the σ interactions along the a axis in $Sr_2Ta_2O_7$ [28] (Fig. 2d) provides the best opportunity for electron and hole mobility. In $Sr_5Ta_4O_{15}$ a zigzag-like connection is less favorable for carrier transport, and $Sr_4Ta_2O_9$ is an extreme case in which the octahedra are physically disconnected.

$SrTa_2O_6$ is the particular example in the series of the prepared catalysts in which TaO_6 units form edge-sharing pairs (Ta_2O_{10}) that are connected with each other by corner sharing (Fig. 2a). The electronic band structure of such compounds has not been as extensively explored as that of perovskites. An attempt to analyze the bandwidth dependence on corner and edge sharing in the perovskite and cadmium halide structures has been made by Burdett and Gramsch [29]. According to their findings, edge-sharing of MO_6 octahedra leads to t_{2g}–e_g separation and formation of even narrower bands, in contrast to the perovskite case, in which t_{2g} and e_g levels overlap and give rise to a relatively broad

band. In our case of the $SrTa_2O_6$ compound, the bottom of the band formed by t_{2g} would correspond to the conduction band. Thus, even though the band gap of $SrTa_2O_6$ is the smallest among the four materials and hydrogen and oxygen production from water is still thermodynamically possible, the width of the conduction band for this compound should be narrower than that of perovskite-related compounds. We would like to emphasize that this explanation is rather rough, because of the lack of systematic studies on the electronic structures of compounds with the same building blocks as $SrTa_2O_6$; therefore we expect exciting outcomes from the band structure computations for these materials.

4. Conclusion

Single-phase samples of $SrTa_2O_6$, $Sr_4Ta_2O_9$, and $Sr_5Ta_4O_{15}$ were successfully synthesized by heat treatment of the PC powder precursors at a reduced temperature. Specimens were characterized by XRD, UV–visible spectroscopy, and measurements of the specific surface areas. The photocatalytic activity of water decomposition by $SrTa_2O_6$, $Sr_4Ta_2O_9$, and $Sr_5Ta_4O_{15}$ (in the presence of NiO as a co-catalyst) was measured and compared against reported data for $Sr_2Ta_2O_7$. A possible relationship between photocatalytic activities and crystal structures of the synthesized compounds was discussed.

Acknowledgment

This work was financially supported by CREST/JST.

References

[1] K. Domen, J.N. Kondo, M. Hara, T. Takata, Bull. Chem. Soc. Jpn. 73 (2000) 1307.
[2] A. Kudo, H. Kato, Chem. Lett. 26 (1997) 867.
[3] T. Ishihara, H. Nishiguchi, K. Fukamachi, Y. Takita, J. Phys. Chem. B 103 (1999) 1.
[4] H. Kato, A. Kudo, J. Phys. Chem. B 105 (2001) 4285.
[5] A. Kudo, H. Kato, S. Nakagawa, J. Phys. Chem. B 104 (2000) 571.
[6] M. Machida, J. Yabunaka, T. Kijima, Chem. Mater. 12 (2000) 812.
[7] A. Kudo, H. Okutomi, H. Kato, Chem. Lett. 29 (2000) 1212.
[8] K. Shimizu, Y. Tsuji, T. Hatamachi, K. Toda, T. Kodama, M. Sato, Y. Kitayama, Phys. Chem. Chem. Phys. 6 (2004) 1064.
[9] P.M. Pechini, US Patent 3330697 (1967).
[10] M. Kakihana, J. Sol-Gel Sci. Technol. 6 (1996) 7.
[11] M. Yoshino, M. Kakihana, W.S. Cho, H. Kato, A. Kudo, Chem. Mater. 14 (2002) 3369.
[12] C.D. Whiston, A.J. Smith, Acta. Crystallogr. 23 (1967) 82.
[13] H. Kato, A. Kudo, Chem. Lett. 28 (1999) 1207.
[14] F. Galasso, L. Katz, Acta. Crystallogr. 14 (1961) 647.
[15] M.T. Caldes, P. Deniard, X.D. Zou, R. Marchand, N. Diot, R. Brec, Micron 32 (2001) 497.
[16] M.V. Paromova, P.P. Leshchenko, L.N. Lykova, L.M. Kovba, Vestn. Mosk. Univ. Khim. 17 (1976) 499.
[17] I. Levin, J.Y. Chan, J.H. Scott, L. Farber, T.A. Vanderah, J.E. Maslar, J. Solid State Chem. 166 (2002) 24.
[18] A. Kudo, K. Sayama, A. Tanaka, K. Asakura, K. Domen, K. Maruya, T. Onishi, J. Catal. 120 (1989) 337.
[19] F. Izumi, T. Ikeda, Mater. Sci. Forum 321–324 (2000) 198.
[20] P.V. Sirotinkin, P.S. Sirotinkin, Z. Neorg. Khim. 38 (1993) 1071.
[21] H.B. Zandbergen, D.J.W. Ijdo, Acta Crystallogr. C 39 (1983) 829.
[22] J. Shannon, L. Katz, Acta Crystallogr. B 26 (1970) 102.
[23] I.D. Brown, D. Altermatt, Acta Crystallogr. B 41 (1985) 244.
[24] M.S. Wrighton, A.B. Ellis, P.T. Wolczanski, D.L. Morse, H.B. Abrahamson, D.S. Ginley, J. Am. Chem. Soc. 98 (1976) 2774.
[25] E.D. Scaife, Solar Energy 25 (1980) 41.
[26] H. Kato, A. Kudo, J. Photochem. Photobiol. A 145 (2001) 129.
[27] H.W. Eng, P.W. Barnes, B.M. Auer, P.M. Woodward, J. Solid State Chem. 175 (2003) 94.
[28] N. Ishizawa, F. Marumo, T. Kawamura, M. Kimura, Acta Crystallogr. B 32 (1976) 2564.
[29] J.K. Burdett, S.A. Gramsch, Inorg. Chem. 33 (1994) 4309.